# Metal-insulator transitions in strained single quantum wells of $Sr_{1-x}La_xVO_3$

K. S. Takahashi,[1,*] J. Iguchi,[2] Y. Tokura,[1,2,3] and M. Kawasaki[1,2]
[1]*RIKEN Center for Emergent Matter Science (CEMS), Wako 351-0198, Japan*
[2]*Department of Applied Physics and Quantum Phase Electronics Center, University of Tokyo, Tokyo 113-8656, Japan*
[3]*Tokyo College, University of Tokyo, Tokyo 113-8656, Japan*

(Received 2 October 2023; accepted 9 January 2024; published 25 January 2024)

Metal-insulator transitions (MITs) are ubiquitous in strongly correlated electron systems. However, there is an unexplored area of study: the artificially confined systems of strained quantum wells that are comprehensively studied in semiconductors for practical device applications. Here we have systematically studied quantum wells of $Sr_{1-x}La_xVO_3$, a compound that evolves from a $3d^1$ metal ($SrVO_3$) to a $3d^2$ Mott insulator ($LaVO_3$). The two-dimensional confinement is shown to enhance the stability of the insulating phase, shifting the critical MIT value of $x$ from $x = 0.82$ for the bulk to around $x = 0.50$ at a thickness of 4 unit cells (u.c.); below 3 u.c. the insulating state merges with the newly emerging $d^1$ Mott insulator state ($x = 0$). The Mott insulator states are further stabilized by a tensile epitaxial strain, presumably due to the enhanced correlation in selectively occupied $d_{xy}$ orbitals. These findings pave the way for exploring Mott physics in an artificially confined system of a strongly correlated electron system.

DOI: 10.1103/PhysRevB.109.035158

## I. INTRODUCTION

Transition-metal oxides endowed with correlated electrons are among the most extensively studied materials for a variety of intriguing properties such as superconductivity, magnetism, multiferroicity, and other versatile properties [1]. The metal-insulator transition (MIT) is one of the most fundamental phenomena in correlated electron systems that can be studied in a systematic way in transition-metal complex oxides [2]. The MIT can be controlled by varying the relative magnitude of the on-site Coulomb interaction $U$ and transfer (hopping) integral $t$ between nearby transition-metal sites in accordance with the Mott-Hubbard scheme [3,4]. Thus such an MIT has been widely studied in complex oxides, chemically substituting cations with ones having different ionic radii and/or valence states, where the one-electron bandwidth and its band filling are respectively controlled. Recently, the studies on MIT have been extended to atomically controlled thin film heterostructures hosting two-dimensional (2D) correlated electron systems [5–8]. Since the decrease in the layer thickness causes a reduction of kinetic energy gain along the out of plane direction, 2D Mott insulator states are more easily realized by the suppression of effective $t$ in ultrathin films.

Our target systems are the ultrathin $Sr_{1-x}La_xVO_3$ films confined between insulating $SrTiO_3$ (STO) layers. One end compound $SrVO_3$ (SVO) with the electron occupation of $3d^1$ is a Pauli paramagnetic metal due to a large $t$ mediated with strong hybridization between the $3d$ and O $2p$ orbitals [2,9]. The counter end compound $LaVO_3$ (LVO) is one of the most prototypical Mott insulators with the electron occupation of $3d^2$ that undergoes a transition to antiferromagnetic and an orbital-ordered phase below 140K due to a large $U$ [10,11]. By substituting La with Sr in LVO or by hole doping, the $d^2$ Mott insulator state is changed into a metallic state at around a composition of $Sr_{0.18}La_{0.82}VO_3$, as reported for bulk crystals [Fig. 4(i)] [10]. As for the confinement effect, the emergence of the Mott-Hubbard gap was revealed in photoemission spectra for SVO films with reducing the thicknesses to 2–3 unit cells (u.c.) through a dimensional crossover around 3–5 u.c. [5,12]. We have recently confirmed this MIT by the electrical transport measurements for SVO single quantum well structures at around 3 u.c. confined with STO barrier layers grown on $(LaAlO_3)_{0.3}(Sr_2AlTaO_6)_{0.7}$ (LSAT) substrates [13]. Such a systematic study of transport for a confined system has become possible since high-quality SVO thin films have been available as manifested by a quite low residual resistivity on the order of $10^{-7}\Omega\,\mathrm{cm}$ for thick films grown by metalorganic gas source molecular beam epitaxy (MOMBE). Electron doping by La substitution of Sr ($Sr_{1-x}La_xVO_3$) is shown to recover a metalliclike conductive state at around $x = 0.17$ for 2 and 3 u.c. heterostructures [13]. In addition, the $d^2$ Mott insulator state on the $LaVO_3$ side might extend into a broader region, reaching approximately $x = 0.2$. The phase diagrams with a MIT in the low $x$ region for such quantum wells are significantly different from those of bulk crystals which are kept metallic up to $x = 0.82$. Thus it is interesting to examine the stability of the $d^2$ Mott insulator phase on the $LaVO_3$ side for more metallic and thicker quantum wells such as 4 and 5 u.c. thick ones.

To scrutinize the MIT in the $Sr_{1-x}La_xVO_3$ system, an interesting approach is to examine the phase diagram for more metallic structures with thicker quantum wells under epitaxial strain. Since the charge dynamics of electrons is anticipated to couple with their orbital and spin degrees of freedom in this $Sr_{1-x}La_xVO_3$ system [14], the concomitant effect of epitaxial

*kei.takahashi@riken.jp

 

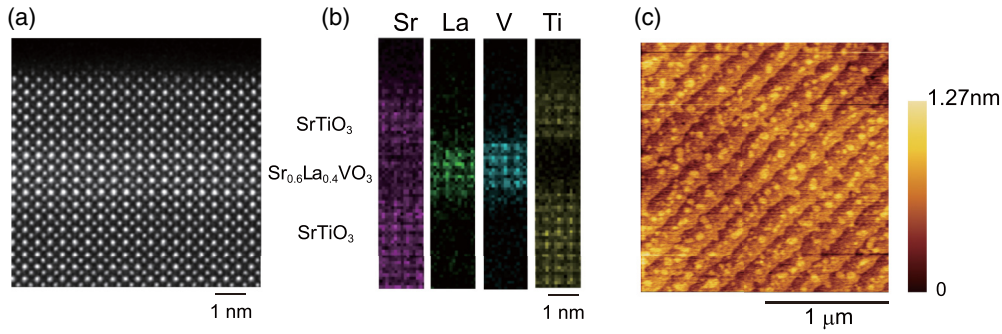


FIG. 1. Structural characterization of $Sr_{1-x}La_xVO_3$ heterostructures. (a) A cross-sectional high-angle annular dark-field scanning transmission electron microscope (HAADF STEM) image taken along the [100] axis for a STO(5 u.c.)/$Sr_{0.4}La_{0.6}VO_3$(4 u.c.)/STO(5 u.c.) heterostructure grown on a STO(001) substrate. (b) The elemental map taken for the $L$ edges of Sr and La and $K$ edges of V and Ti atoms with an energy dispersive x-ray spectrometry (EDX) at the same area in (a). (c) An atomic force microscope (AFM) image ($2 \times 2\,\mu m^2$) for the surface of the same sample.

strain and confinement will provide electronic phase diagrams with rich features. Previously, the strain effect was studied for thick films of the end compound LVO grown on STO and $DyScO_3$ substrates to discuss the effect of epitaxial strain on the ordering temperatures for orbitals and spins [15,16]. However, such combined effects of confinement and epitaxial strain have not been systematically investigated for the solid solution films of $Sr_{1-x}La_xVO_3$.

In this study, we have fabricated $Sr_{1-x}La_xVO_3$ ultrathin films with the thicknesses of 2, 3, 4, and 5 u.c. on STO and LSAT substrates. The ground state of nondoped SVO with thicknesses of 2 and 3 u.c. is found to be a $d^1$ Mott insulator, while those with 4 and 5 u.c. are metal on the verge of MIT. Thus such a tiny perturbation as doping and epitaxial strain modifies the phase stability as probed by the resistivity measurements in this study. The phase diagram in the thickness ($z$)–filling ($x$) plane indicates the enhanced stability of the $d^1$ and $d^2$ Mott insulator state by the 2D confinement as well as by the large tensile strain on STO. Unlike naturally made 2D multilayer systems, such as the Ruddlesden-Popper series with finite coupling between layers [17], artificially made single quantum well structures can be a unique playground for examining the intrinsic properties of isolated 2D correlated electron systems.

## II. EXPERIMENT

Thin film heterostructures were grown by MOMBE [18–20] with successively depositing a STO buffer layer (5 u.c.), a $Sr_{1-x}La_xVO_3$ layer ($z$ u.c.), and a STO capping layer (5 u.c.) on either the STO or LSAT substrate. The substrate temperature for the buffer STO layer was set at 900 °C and that for $Sr_{1-x}La_xVO_3$ and the capping STO layers was at 800 °C. After the deposition, the heterostructures were *ex situ* annealed at 250 °C in air to fully oxidize the samples. The details of the growth conditions are described in our previous paper [13]. The structural characterizations have been performed with atomic force microscopy (AFM), high-angle annular dark-field scanning transmission electron microscopy (HAADF STEM), and energy dispersive x-ray spectroscopy (EDX). Figures 1(a) and 1(b) are the cross-sectional HAADF STEM image and EDX intensity maps for constituent elements, respectively, for a $Sr_{0.4}La_{0.6}VO_3$ (4 u.c.) heterostructure grown on STO (001). The structure is verified to agree very well with the design. A typical AFM image of the sample is shown in Fig. 1(c); it exhibits step and terrace structures with a step height of 4 Å. Such atomically regulated structures are prerequisite for discussing the intrinsic electrical transport properties in single quantum well structures.

## III. RESULTS AND DISCUSSION

Let us first examine the confinement and epitaxial strain effects for the $d^1$ end member SVO. Figure 2 shows the temperature dependences of the resistivity for single quantum wells with various SVO thicknesses of $z$ u.c., namely, STO (5 u.c.)/SVO($z$ u.c.)/STO(5 u.c.) on STO [panel (a)] and LSAT [panel (b)]. Here, we chose cubic STO ($a = 3.905$Å) and LSAT ($a = 3.868$Å) as substrates, giving a lattice mismatch of +1.6% and +0.7%, respectively, with cubic SVO (3.842 Å). Therefore, SVO on STO is under large tensile strain, while that on LSAT is nearly lattice matched. With the thickness variation, one can find the MIT takes place at around $z = 3$ u.c. on both substrates. The value of resistivity for each

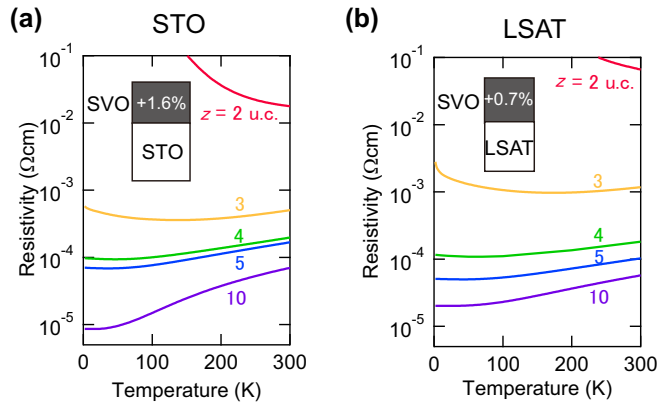


FIG. 2. Transport properties of $SrVO_3$ films with various thicknesses. Temperature dependence of resistivity for STO(5 u.c.)/SVO ($z$ u.c.)/STO(5 u.c.) heterostructures grown on LSAT (001) (a) and STO(001) (b) substrates.

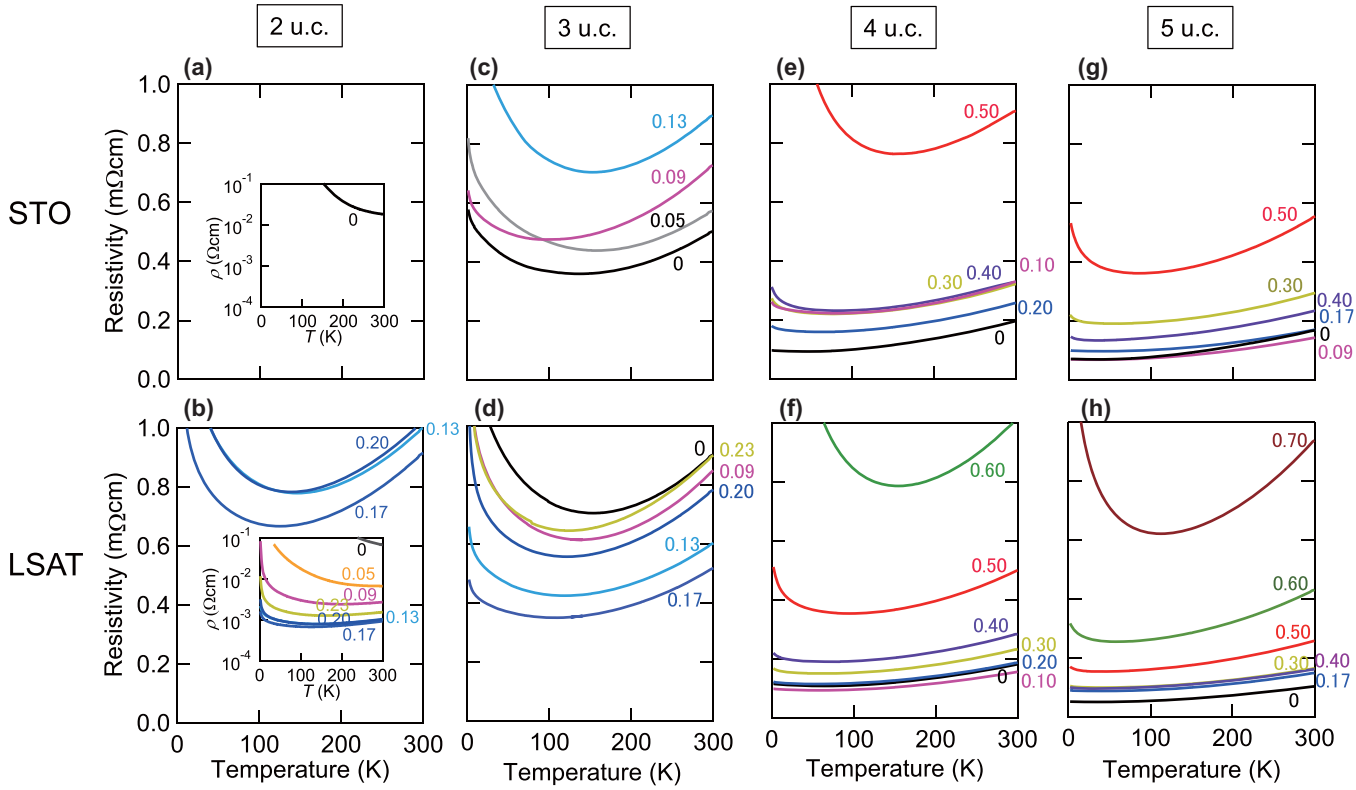


FIG. 3. Transport properties of $Sr_{1-x}La_xVO_3$ heterostructures with various thicknesses on two different substrates. The samples are STO(5 u.c.)/$Sr_{1-x}La_xVO_3$($z$ u.c.)/STO(5 u.c.) heterostructures with various $x$ for $z = 2$ u.c. (a), 3 u.c. (c), 4 u.c. (e), and 5 u.c. (g) on LSAT(001) substrates and for $z = 2$ u.c. (b), 3 u.c. (d), 4 u.c. (f), and 5 u.c. (h) on STO(001) substrates.

thickness of the SVO layer on LSAT is close to or slightly larger than that on STO except for the 5 u.c. sample. Thus, in the case of pristine SVO, it is hard to identify a clear tendency of strain effect from the resistivity data alone. We found that the crystalline quality of SVO on STO remains excellent up to 10 u.c., while the sample quality obviously becomes worse for samples thicker than 20 u.c. on STO judging from the AFM analysis. This contrasts with the fact that a thick film ($z = 190$ u.c.) on a better lattice matched LSAT substrate has high crystalline quality and the resistivity at low temperatures reaches down to the order of $10^{-7}\,\Omega\,\mathrm{cm}$ [13]. Thus we will discuss only samples with thicknesses of 2–10 u.c. in this study.

Figure 3 shows the temperature dependence of resistivities for $Sr_{1-x}La_xVO_3$ layers with thicknesses of 2 [panels (a,b)], 3 [panels (c,d)], 4 [panels (e,f)], and 5 u.c. [panels (g,h)] on STO and LSAT, respectively. One can find a clear difference between the data for thicknesses of 2 and 3 u.c. and those for 4 and 5 u.c. By the strong confinement below 3 u.c., the 2D $d^1$ Mott insulator state appears for SVO on both substrates. On the LSAT substrate as shown in Figs. 3(b) and 3(d), the resistivity decreases by the electron doping with substituting Sr with La, reaching a metallicke state at around $x = 0.17$. We conclude that the electron doping causes the collapse of the 2D $d^1$ Mott insulator state [13]. In stark contrast, such collapse of the Mott insulator state is not observed in the quantum wells of 2 and 3 u.c. on STO as respectively shown in Figs. 3(a) and 3(c), and rather the resistivity keeps increasing with electron doping. Only the 2 u.c. sample of SVO ($x = 0$) on STO is shown in Fig. 3(a), as the resistivities of La-substituted samples are too high to perform four-terminal measurements. When $x$ was raised from 0 to 0.17, a gradual increase of the resistance by an order of magnitude was observed by two terminal measurements. The origin of such a rather monotonous increase in resistivity upon the La substitutions for the quantum wells of 2 u.c. and 3 u.c. on STO with little tendency of Mott insulator collapse may be ascribed to the overwhelming localization effect stemming from the doped $d^2$ electron correlation; it possibly causes the charge/orbital ordering that may be critically dependent on the electron doping $x$, the low-dimensional confinement effect, and the strained lattice form, leading to the resistivity increase with $x$ as observed.

In the case of 4 and 5 u.c. [Figs. 3(e)–3(h)], all resistivity curves for $x \leqslant 0.4$ show metallic behaviors, indicating the metallic state is kept even under the confinement down to 4 and 5 u.c. at such a doping level. The resistivity monotonically increases with increasing $x$ and such metallic states eventually transform into insulating states at around $x = 0.5-0.7$. Therefore, due to the loss of the kinetic energy gain along the out of plane direction in such ultrathin layers, the region of the $d^2$ Mott insulator state is expanded to a lower doping region from $x = 0.82$ in the bulk 3D case. In fact, one can also find a tendency that the critical concentration $x$ for the MIT is lower for the 4 u.c. sample than for the 5 u.c. ones on each substrate. In addition, the effect of tensile strain is seen as a trend of lower critical concentration $x$ on STO than on LSAT. Besides the systematic variation in the critical $x$ of MIT, $T^2$

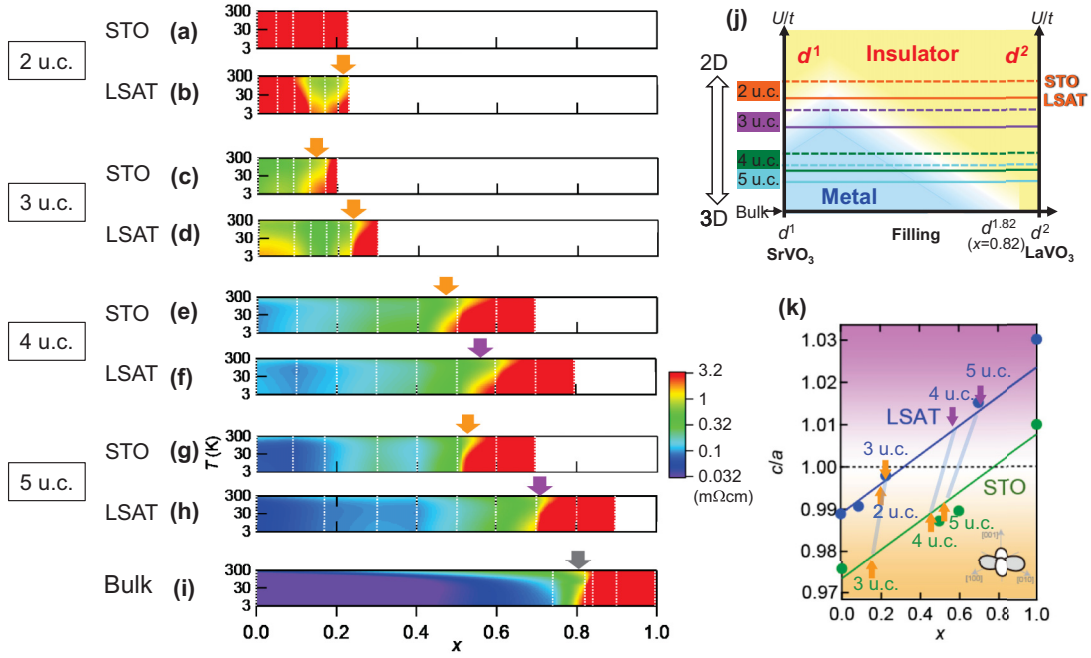


FIG. 4. Phase diagrams of $Sr_{1-x}La_xVO_3$ heterostructures and bulk single crystals. Contour plot of resistivity $\rho(T)$ in logarithmic scale with the color code shown in the middle top panel for $Sr_{1-x}La_xVO_3$ heterostructures with the respective thicknesses of 2, 3, 4, and 5 u.c. on STO (a,c,e,g) and on LSAT (b,d,f,h) as well as that of bulk single crystals (i) [21,22]. The examined samples are indicated by white dotted lines. The critical $x$ positions between metallic and $d^2$ Mott insulator states are indicated by arrows in Figs. 4(b)–4(i) with purple for a compressive strain, orange for a tensile one, and black for a strain free of bulk crystals. The top right panel (j) is a schematic phase diagram of the metal-insulator transition based on the Hubbard model in the plane of $U/t$ and filling ($x$) for this $Sr_{1-x}La_xVO_3$ system. The phase diagram of quantum well structures can be nicely expressed on different $U/t$ positions depending on the thickness and strain. The bottom right panel (k) is the tetragonality $c/a$ as a function of $x$ for strained $Sr_{1-x}La_xVO_3$ films on STO and LSAT substrates. The compositions of the metal-insulator transition are indicated with arrows for quantum well samples with various thicknesses, which correspond to the arrows in (b)–(h).

dependences were commonly observed in the resistivity curves for all the metallic samples as shown in Fig. 5, indicating that the scattering mechanism is dominated by the electron-electron interaction. We briefly discuss such temperature dependence of resistivity in Appendix A in relation with the strength of the correlation effect.

To gain an overview on the dependence of the MIT on the thickness and strain, we show contour plots of the resistivity in temperature ($T$)–filling ($x$) planes in Fig. 4. The plot for bulk single crystals is shown for comparison in Fig. 4(i) [21,22]. Since the MIT in correlated electron oxides tends to occur at a critical resistivity value corresponding to the Ioffe-Regel limit of $\sim$1 m$\Omega$ cm, the logarithmic color scale is adjusted to have yellow there. At a glance, one can see the critical concentration $x$ for the MIT decreases as the thickness decreases from bulk crystals through 5 to 4 u.c. Below 3 u.c., such insulator regions seem to invade down to $x = 0.2$ and finally to merge with the $d^1$ Mott insulator states for 2 u.c. Considering these results, a MIT phase diagram can be schematically drawn as Fig. 4(j) in the plane of $U/t$ and filling ($x$) for this single quantum well $Sr_{1-x}La_xVO_3$ system. As the lowest limit of $U/t$, the phase diagram of bulk $Sr_{1-x}La_xVO_3$ crystals is shown, where one can find SVO ($x = 0$) as the $d^1$ metallic state, LVO ($x = 1$) as the $d^2$ Mott insulator state, and the MIT at around $x = 0.82$. The confinement (reduction in the quantum well thickness $z$) effect can be projected as the increase in $U/t$ due to the reduction of kinetic energy gain. For the end compound SVO ($x = 0$), the $d^1$ Mott insulator state emerges for quantum wells thinner than 3 u.c., while the 4 and 5 u.c. ones stay within a metallic regime below the critical boundary with the expanded $d^2$ Mott insulator state. Thus the phase diagrams of $Sr_{1-x}La_xVO_3$ with thicknesses of 2 and 3 u.c. correspond to the upper regions in Fig. 4(j), reproducing the metallic-like phase sandwiched between the $d^1$ and $d^2$ Mott insulator states. Likewise, the lower regions correspond to those with thicknesses of 4 and 5 u.c. Namely, by reducing the thickness $z$ (increasing the $U/t$), critical $x$ between the metallic and $d^2$ Mott insulator states shifts from $x = 0.82$ in the bulk crystal to lower $x$ for higher $U/t$, around $x = 0.55 - 0.70$ for 5 u.c., and $x = 0.50 - 0.60$ for 4 u.c.

We can also discuss the effect of epitaxial strain using these phase diagrams. Assuming tetragonal distortion in $Sr_{1-x}La_xVO_3$ quantum well structures, useful lattice parameters for considering orbital occupancy are the tetragonality $c/a$ with $a = b$, the ratio of out of plane to in-plane lattice constants, in fully strained pseudomorphic films. Since it is not practically possible to evaluate the actual lattice parameters for these ultrathin quantum wells, we fabricated a series of thick ($z = 20-50$ u.c.) films on both STO and LSAT substrates and confirmed fully strained structure with in-plane lattice constants $a$ identical to those of the substrates. The solid symbols in Fig. 4(k) correspond to the experimentally

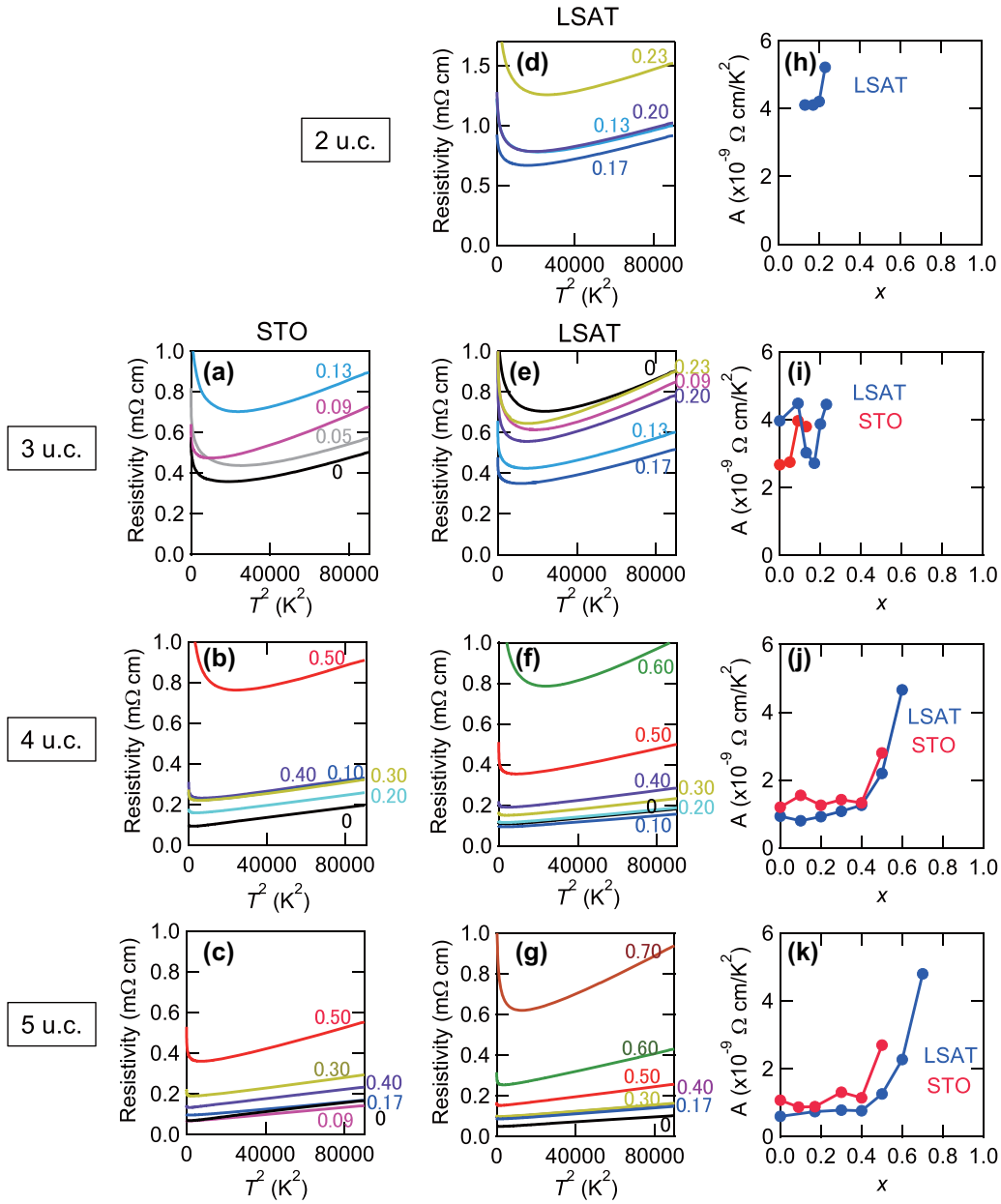


FIG. 5. Resistivity versus $T^2$ for $Sr_{1-x}La_xVO_3$ single quantum wells. The samples are STO(5 u.c.)/$Sr_{1-x}La_xVO_3$($z$ u.c.)/STO(5 u.c.) heterostructures with various $x$ for $z = 3$ u.c. (a), 4 u.c. (b), and 5 u.c. (c) on STO(001) substrates and for $z = 2$ u.c. (d), 3 u.c. (e), 4 u.c. (f), and 5 u.c. (g) on LSAT(001) substrates. Corresponding to these data, the $x$ dependences of $A$ that is the slope of the resistivity versus $T^2$ of the quantum wells are shown for $z = 2$ u.c. (h) on LSAT, 3 u.c. (i), 4 u.c. (j), and 5 u.c. (k) on LSAT and STO(001) substrates.

deduced $c/a$ as a function of $x$ for the thick films on LSAT (blue) and STO (green) substrates. The straight lines are expected $c/a$ values deduced assuming Vegard's law and elastic deformation as detailed in Appendix B. As can be seen, the strain of epitaxial films changes from a tensile strain to a compressive one with increasing $x$. The boundaries between tensile and compressive strain states are located around $x = 0.8$ on STO and 0.3 on LSAT.

To make a clearer comparison of MIT and strain, we indicate the critical $x$ positions between the metallic and $d^2$ Mott insulator states by arrows in Figs. 4(b)–4(i) and 4(k) with purple for a compressive strain, orange for a tensile one, and black for a strain free of bulk crystals. In the case of 4 and 5 u.c., the critical $x$ is systematically lower for $Sr_{1-x}La_xVO_3$ quantum wells on STO under a tensile strain state than those on LSAT under a compressive strain state. As for the 2 and 3 u.c., MITs occur at much lower $x$. The critical value $x$ of MIT at 3 u.c. shifts from $x = 0.23$ on LSAT to $x = 0.15$ on STO. As for 2 u.c. samples, the $d^2$ and $d^1$ Mott insulator states eventually merge on STO without the appearance of the metalliclike state that is observed in a narrow region around $x = 0.17$ on LSAT.

Such strain-dependent stabilization of the $d^2$ Mott insulator state should be related with the selective occupation of Ti $t_{2g}$ orbitals. In a bulk crystal of $LaVO_3$, the lattice at 300 K is nearly cubic with $a = 3.923$ Å (in a pseudocubic setting)

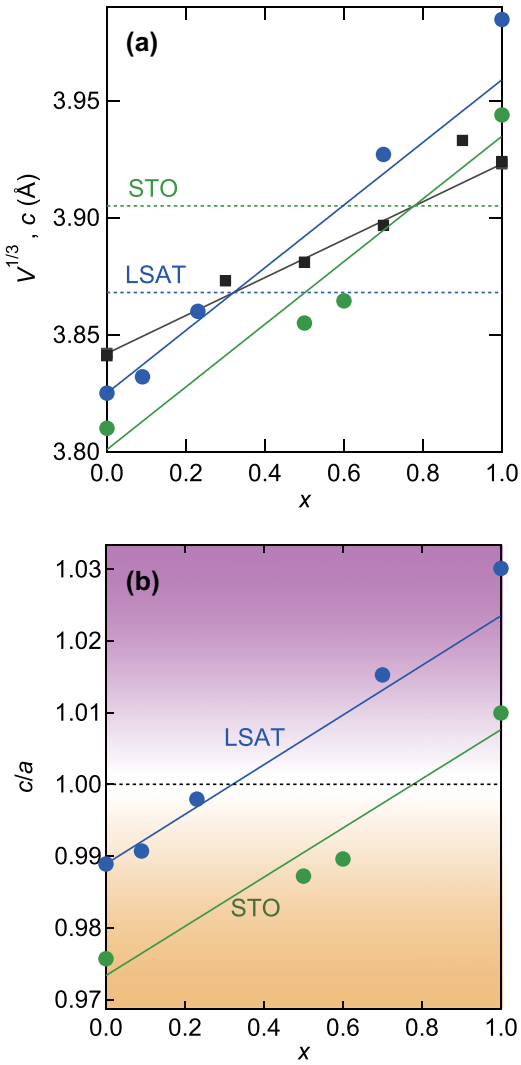


FIG. 6. Epitaxial strain in $Sr_{1-x}La_xVO_3$ films. (a) Lattice parameters as a function of $x$ for $Sr_{1-x}La_xVO_3$. Circles: out of plane lattice constants ($c$) of fully strained $Sr_{1-x}La_xVO_3$ epitaxial films on STO (green) and LSAT (blue) substrates. Black squares: lattice constants of $Sr_{1-x}La_xVO_3$ bulk samples with a pseudocubic lattice definition (1/3 power of cell volume). Black line represents Vegard's law interpolating the values for SVO and LVO single crystals. Green and blue lines are merely guides for the eyes, which are deduced form the black line assuming a Poisson's ratio of 0.25 with a full epitaxial strain on STO and LSAT substrates, respectively. (b) The vertical axis is transformed to the tetragonality $c/a$ for the epitaxial films on STO and LSAT.

and it goes to a nearly tetragonal lattice with $c/a = 0.983$ ($a \approx b = 3.945$ Å and $c = 3.880$ Å) at the antiferromagnetic and orbital-ordered state at low temperatures [11,23]. Here, it is elucidated that one $d$ electron preferentially occupies the $d_{xy}$ orbital and the other $d$ electron does alternately $d_{yz}$ and $d_{zx}$ orbitals in the $ab$ plane with a checkerboard pattern. In previous studies, Meley *et al.* found that a large tensile strain ($c/a = 0.988$ at 300 K and 0.984 at low temperature below the phase transition) in a $LaVO_3$ film on a $DyScO_3$ substrate lowers the $d_{xy}$ energy level and increases the orbital ordering temperature of the $d_{yz}/d_{zx}$ orbitals, while a slight compressive strain on STO ($c/a = 1.006$ at 300 K) does not change the property of orbital ordering so much from those of bulk crystal [16]. Therefore, tensile strain in the present quantum wells is expected to enhance the electron correlation not only by the confinement but also by the stronger orbital polarization in $d_{xy}$ as shown in the inset of Fig. 4(k). Such lowering of the $d_{xy}$ orbital energy level tends to enhance the stability of the $d^2$ Mott insulator state against hole doping; this orbital-dependent stability pushes the MIT critical $x$ (or hole doping $p = 1 - x$) toward lower (higher) values in the tensile strained quantum wells on STO than the compressive strained ones on LSAT.

## IV. CONCLUSIONS

In conclusion, we have studied the phase diagram of ultrathin $Sr_{1-x}La_xVO_3$ quantum wells grown by MOMBE. By reducing the thickness of $Sr_{1-x}La_xVO_3$, the $d^2$ Mott insulator state originating from $LaVO_3$ ($x = 1$) is more stabilized to the lower $x$ region and finally merges with the 2D confinement induced $d^1$ Mott insulator state originating from $SrVO_3$ ($x = 0$). The overall feature is well understood, as the stronger confinement leads to a larger $U/t$; the electron correlation overcomes the kinetic energy gain of electron transfer by the suppression of that along the thickness direction. The tensile strain imposed to the quantum well tends to stabilize the insulator state, possibly due to the selective occupation or polarization of $3d_{xy}$ orbitals of V ions causing the stronger electron correlation. This study has clarified a prototypical electronic phase diagram of a $d^{1+x}$ ($0 \leqslant x \leqslant 1$) system realized in $Sr_{1-x}La_xVO_3$ as functions of confinement and epitaxial strain, leading to deeper understanding of the correlated electron quantum well for exploring electronic phases.

## ACKNOWLEDGMENTS

This work was partly supported by JSPS KAKENHI (Grants No. 22H04958 and No. 23H01857) and the Mitsubishi Foundation.

## APPENDIX A: FERMI LIQUID BEHAVIOR SEEN IN TEMPERATURE DEPENDENCE OF RESISTIVITY FOR STRAINED SINGLE QUANTUM WELLS OF $Sr_{1-x}La_xVO_3$

It is known that the resistivity ($\rho$) of a Fermi liquid follows a quadratic temperature dependence expressed as $\rho = \rho_0 + AT^2$ at low temperatures, where the strength of electron-electron interaction appears to enhance $A$. When the electron system approaches a quantum critical point, non-Fermi liquid behavior is often observed as a deviation from the $T^2$ dependence. One of the famous examples is a $T$-linear dependence in a wide temperature range for high-temperature superconducting cuprates that face the quantum critical point with antiferromagnetic phases. In the case of $Sr_{1-x}La_xVO_3$ bulk crystals, $T^{1.5}$ dependence was reported in the metallic region near the MIT boundary ($x = 0.7$–$0.8$) by Inaba *et al.* [10]. They argued that such temperature dependence may originate from the strong antiferromagnetic spin fluctuation possibly due to the proximity with the end compound of $LaVO_3$ with antiferromagnetic ordering.

In Fig. 5, the resistivity of $Sr_{1-x}La_xVO_3$ quantum wells is shown as a function of $T^2$ with various thicknesses on two different substrates. Interestingly, all the curves with various compositions follow the $T^2$ dependence even in the region close to the Mott insulator transitions with largest $x$, although the coefficient $A$ steeply enhances towards the transitions as shown in the $x$ dependences of $A$. These results suggest that the emergence of spin fluctuation does not appear even though the quantum well samples approach the $d^2$ Mott insulator state. Presumably it is due to the destabilization of long-range antiferromagnetic ordering for the $d^2$ Mott insulator state because of the confinement effect, limiting the number of spins along the out of plane direction.

## APPENDIX B: EPITAXIAL STRAIN IN $Sr_{1-x}La_xVO_3$ FILMS

Since the intensity of x-ray diffraction peaks is too weak to determine the lattice constants for very thin quantum wells, we estimate them from those of fully strained thick heterostructures ($z = 20-50$ u.c.) and compare them with the trend of bulk crystals. Solid circles in Fig. 6 are the data of out of plane lattice constants ($c$) for fully strained thick films on STO (green) and LSAT (blue) substrates. Taking into account the lattice constant of cubic SVO as 3.842 Å and that of orthorhombic LVO with a pseudocubic lattice definition as 3.923 Å, the lattice constant ($V^{1/3}$) of $Sr_{1-x}La_xVO_3$ can be estimated as $a = 3.842 + 0.081x$ if it follows Vegard's law. As shown in Fig. 6(a), the data of lattice constants for bulk single and polycrystals of $Sr_{1-x}La_xVO_3$ (black squares) agree well with this Vegard's law (black line) [11,22,24]. Assuming the coherent epitaxy keeping the same in-plane lattice constant with the substrate and the Poisson ratio as 0.25, out of plane lattice constants of $Sr_{1-x}La_xVO_3$ films can be calculated as the green and blue lines on STO and LSAT, respectively, from the black line. The experimentally deduced lattice constants (solid circles) fit well with the calculated lines as expected. Since the epitaxial strain should make an impact on the energy levels of $t_{2g}$ orbitals, it is useful to convert the lattice constants to the tetragonality $c/a$ as a function of $x$ as shown in Fig. 6(b). The boundary from tensile to compressive strain locates at around $x = 0.8$ and 0.3 for the films on STO and LSAT, respectively.


[1] Y. Tokura, Correlated-electron physics in transition-metal oxides, Phys. Today **56**, 50 (2003).

[2] M. Imada, Fujimori, and Y. Tokura, Metal-insulator transitions, Rev. Mod. Phys. **70**, 1039 (1998).

[3] J. Hubbard, Electron correlations in narrow energy bands, Proc. R. Soc. London, Ser. A **276**, 238 (1963).

[4] N. F. Mott, *Metal-Insulator Transitions* (Taylor and Francis, London, 1990).

[5] K. Yoshimatsu, T. Okabe, H. Kumigashira, S. Okamoto, S. Aizaki, A. Fujimori, and M. Oshima, Dimensional-crossover-driven metal-insulator transition in $SrVO_3$ ultrathin films, Phys. Rev. Lett. **104**, 147601 (2010).

[6] K. Yoshimatsu, K. Horiba, H. Kumigashira, T. Yoshida, A. Fujimori, and M. Oshima, Metallic quantum well states in artificial structures of strongly correlated oxide, Science **333**, 319 (2011).

[7] S. G. Jeong, T. Min, S. Woo, J. Kim, Y.-Q. Zhang, S. W. Cho, J. Son, Y.-M. Kim, J. H. Han, S. Park, H. Y. Jeong, H. Ohta, S. Lee, T. W. Noh, J. Lee, and W. S. Choi, Phase instability and dimensional crossover in artificial oxide crystal, Phys. Rev. Lett. **124**, 026401 (2020).

[8] R. Scherwitzl, P. Zubko, C. Lichtensteiger, and J.-M. Triscone, Electric-field tuning of the metal-insulator transition in ultrathin films of $LaNiO_3$, Appl. Phys. Lett. **95**, 222114 (2009).

[9] I. H. Inoue, I. Hase, Y. Aiura, A. Fujimori, Y. Haruyama, T. Maruyama, and Y. Nishihara, Systematic development of the spectral function in the $3d^1$ Mott-Hubbard system $Ca_{1-x}Sr_xVO_3$, Phys. Rev. Lett. **74**, 2539 (1995).

[10] F. Inaba, T. Arima, T. Ishikawa, T. Katsufuji, and Y. Tokura, Change of electronic properties on the doping-induced insulator-metal transition in $La_{1-x}Sr_xVO_3$, Phys. Rev. B **52**, R2221 (1995).

[11] S. Miyasaka, T. Okuda, and Y. Tokura, Critical behavior of metal-insulator transition in $La_{1-x}Sr_xVO_3$, Phys. Rev. Lett. **85**, 5388 (2000).

[12] M. Kobayashi, K. Yoshimatsu, T. Mitsuhashi, M. Kitamura, E. Sakai, R. Yukawa, M. Minohara, A. Fujimori, K. Horiba, and H. Kumigashira, Emergence of quantum critical behavior in metallic quantum-well states of strongly correlated oxides, Sci. Rep. **7**, 16621 (2017).

[13] K. S. Takahashi, Y. Tokura, and M. Kawasaki, Metal–insulator transitions in dimensionality controlled $La_xSr_{1-x}VO_3$ films, APL Mater. **10**, 111114 (2022).

[14] S. Miyasaka, Y. Okimoto, and Y. Tokura, Anisotropy of Mott–Hubbard gap transitions due to spin and orbital ordering in $LaVO_3$ and $YVO_3$, J. Phys. Soc. Jpn. **71**, 2086 (2002).

[15] H. Meley, L. O. Karandeep, J. de Bruijckere, D. T. L. Alexander, J.-M. Triscone, Ph. Ghosez, and S. Gariglio, Structural analysis of $LaVO_3$ thin films under epitaxial strain, APL Mater. **6**, 046102 (2018).

[16] H. Meley, M. Tran, J. Teyssier, J. A. Krieger, T. Prokscha, A. Suter, Z. Salman, M. Viret, D. van der Marel, and S. Gariglio, Strain tuning of interorbital correlations in $LaVO_3$ thin films, Phys. Rev. B **103**, 125112 (2021).

[17] J. Matsuno, Y. Okimoto, M. Kawasaki, and Y. Tokura, Synthesis and electronic structure of epitaxially stabilized $Sr_{2-x}La_xVO_4$ ($0 \leqslant x \leqslant 1$) thin films, Appl. Phys. Lett. **82**, 194 (2003).

[18] J. Son, P. Moetakef, B Jalan, O. Bierwagen, N. J. Wright, R. Engel-Herbert, and S Stemmer, Epitaxial $SrTiO_3$ films with electron mobilities exceeding 30, 000 $cm^2\,V^{-1}\,s^{-1}$, Nat. Mater. **9**, 482 (2010).

[19] M. Brahlek, A. S. Gupta, J. Lapano, J. Roth, H.-T. Zhang, L. Zhang, R. Haislmaier, and R. Engel-Herbert, Frontiers in the growth of complex oxide thin Films: Past, present, and future of hybrid MBE, Adv. Funct. Mater. **28**, 1702772 (2017).

[20] M. Brahlek, L. Zhang, H.-T. Zhang, J. Lapano, L. R. Dedon, L. W. Martin, and R. Engel-Herbert, Mapping growth windows in quaternary perovskite oxide systems by hybrid molecular beam epitaxy, Appl. Phys. Lett. **109**, 101903 (2016).

[21] M. Uchida, K. Oishi, M. Matsuo, W. Koshibae, Y. Onose, M. Mori, J. Fujioka, S. Miyasaka, S. Maekawa, and Y. Tokura, Thermoelectric response in the incoherent transport region near Mott transition: The case study of $La_{1-x}Sr_xVO_3$, Phys. Rev. B **83**, 165127 (2011).

[22] I. H. Inoue, O. Goto, H. Makino, N. E. Hussey, and M. Ishikawa, Bandwidth control in a perovskite-type $3d^1$-correlated metal $Ca_{1-x}Sr_xVO_3$. I. Evolution of the electronic properties and effective mass, Phys. Rev. B **58**, 4372 (1998).

[23] P. Bordet, C. Chaillout, M. Marezio, Q. Huang, A. Santoro, S.-W. Cheong, H. Takagi, C. S. Oglesby, and B. Batlogg, Structural aspects of the crystallographic-magnetic transition in $LaVO_3$ around 140 K, J. Solid State Chem. **106**, 253 (1993).

[24] C. Y. Liu, S. Y. Tsai, C. T. Ni, and K. Z. Fung, Effect of strontium-doped lanthanum vanadate on crystal structure, conductivity and vanadium valence state of a $La_{1-x}Sr_xVO_3$ anode in a reducing environment, J. Electron. Mater. **46**, 2301 (2017).